Ultrahigh-frequency microwave phase shifts mediated by ultrafast dynamics in quantum-dot semiconductor optical amplifiers

Chen, Yaohui; Mørk, Jesper

Published in:
I E E E Photonics Technology Letters

Link to article, DOI:
10.1109/LPT.2010.2047851

Publication date:
2010

Document Version
Publisher's PDF, also known as Version of record

Ultrahigh-Frequency Microwave Phase Shifts Mediated by Ultrafast Dynamics in Quantum-Dot Semiconductor Optical Amplifiers

Yaohui Chen and Jesper Mørk

***Abstract*—We present a novel scheme to achieve tunable microwave phase shifts at frequencies exceeding 100 GHz based on wavelength conversion induced by high-speed cross-gain modulation in quantum-dot semiconductor optical amplifiers.**

***Index Terms*—Cross-gain modulation (XGM), quantum dot (QD), semiconductor optical amplifiers (SOAs), wavelength conversion.**

I. Introduction

CONTROLLABLE slow and fast light has been experimentally demonstrated in different active semiconductor waveguide devices at room temperature by exploiting the effect of coherent population oscillations (CPOs) [1]–[3]. From an application point of view, it is of significant interest to realize an optically fed microwave phase shifter based on semiconductor devices, such as semiconductor optical amplifier (SOA), with a variable phase shift range of 2π at gigahertz modulation frequencies. SOA-based phase shifters investigated so far rely on dynamical gain gratings mediated by temporal modulation of the total carrier density in a single wavelength configuration [1]–[5]. The corresponding bandwidth is thus limited by the inverse of the carrier lifetime, i.e., typically on the order of a few to several gigahertz under forward bias. Different approaches towards alleviating the bandwidth limitation have been reported [4], [5]. An alternative configuration is to use cross-gain modulation (XGM)-based wavelength conversion in a distributed-feedback (DFB) laser [6]. Recent calculations and experiments indicate that quantum dot (QD)-based devices are good candidates for high-speed optical signal processing due to the unique ultrafast intersubband carrier dynamics between discrete QD bound states [7]–[11]. In addition to four-wave mixing (FWM)-based high-speed wavelength conversion (>25 GHz) [11], small signal XGM up to 40 GHz in QD SOAs has been experimentally and theoretically demonstrated by increasing the current injection and suppressing the total carrier density depletion [10]. We here propose a dual-wavelength-configured phase shifter based on dynamic gain gratings induced by high-speed XGM in QD SOAs. In contrast to the usual configuration involving a weak probe and strong pump, this concept utilizes the two-wave competition phenomenon [12], namely the strong interaction between two waves with comparable magnitude, caused by XGM via fast intersubband effects in QDs under a high current injection. The main new results compared to previous works are to numerically demonstrate the potential of QD SOAs for this new application as a simple and compact ~180° broadband microwave phase shifter working at frequencies beyond 100 GHz. In addition, this configuration allows an alternative way of characterizing ultrafast QD intraband dynamics.

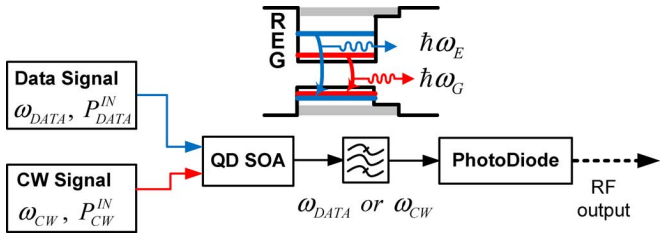

Fig. 1. Configuration of wavelength up-conversion based on XGM in QD SOAs. Inset is a schematic diagram depicting the QD energy levels.

II. Principle of Operation and Modeling

Fig. 1(a) shows the considered wavelength up-conversion configuration based on QD SOAs. It is similar to the small-signal XGM configuration in [12] with a sine-modulated data signal, at optical frequency ω_{DATA}, as input (given by $P^{\mathrm{IN}}_{\mathrm{DATA}}\left[1+m_0\mathrm{Cos}(2\pi ft)\right]$, where $P^{\mathrm{IN}}_{\mathrm{DATA}}$, m_0, and f are input power, modulation index, and modulation frequency). The data signal will modulate the gain of the SOA and thus in turn XGM in the amplifier will transfer the modulation to the copropagating continuous-wave (CW) signal at optical frequency ω_{CW} as an XGM converted signal with an inverse pattern. For simplicity, by ideal flat-top selective optical bandpass filtering, the output intensity envelope centered around ω_{DATA} and ω_{CW} can be detected in the form of $P^{\mathrm{OUT}}_X\left[1+m^{\mathrm{OUT}}_X\mathrm{Cos}\left(2\pi ft+\varphi^{\mathrm{OUT}}_X\right)\right]$. Here, P^{OUT}_X, m^{OUT}_X, and φ^{OUT}_X ($X=\mathrm{CW},\mathrm{DATA}$) are the mean output optical intensity, modulation index, and radio-frequency (RF) phase shift at the given optical frequency. The corresponding RF optical gain is in the form of $P^{\mathrm{OUT}}_X m^{\mathrm{OUT}}_X/\left(P^{\mathrm{IN}}_{\mathrm{DATA}}m_0\right)$. Note that there are two main changes compared to previous results. First, the optical frequencies of the data signal ($\omega_{\mathrm{DATA}}=\omega_E$) and CW signal ($\omega_{\mathrm{CW}}=\omega_G$) are chosen corresponding to

Manuscript received December 31, 2009; revised March 03, 2010; accepted April 02, 2010. Date of publication April 15, 2010; date of current version June 03, 2010. This work was supported by the FP7 GOSPEL project financed by the European Commission, by the QUEST project financed by the Danish Research Councils, and by the NATEC Centre funded by VILLUM FONDEN.

The authors are with DTU Fotonik, Department of Photonics Engineering, Technical University of Denmark, DK-2800, Kgs. Lyngby, Denmark (e-mail: yach@fotonik.dtu.dk; jesm@fotonik.dtu.dk).

Color versions of one or more of the figures in this letter are available online at http://ieeexplore.ieee.org.

Digital Object Identifier 10.1109/LPT.2010.2047851

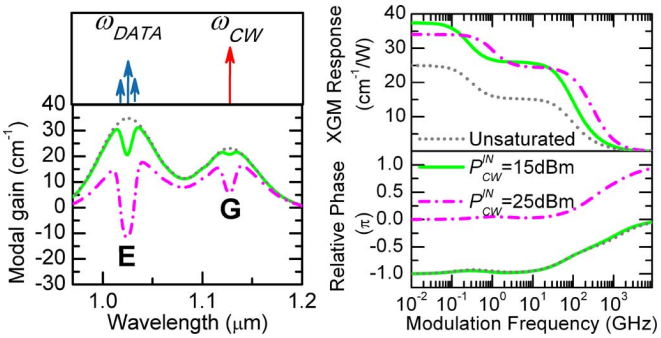

Fig. 2. Calculated modal gain profile for the up-conversion scheme in QD SOAs at a strong current density (10 kA/cm^2) for different input CW power, $P^{\mathrm{IN}}_{\mathrm{CW}}$. (Left) Static spectral modal gain. (Right) XGM response and relative phase. Input data signal is set to $P^{\mathrm{IN}}_{\mathrm{DATA}} = 1$ mW with 20% modulation index.

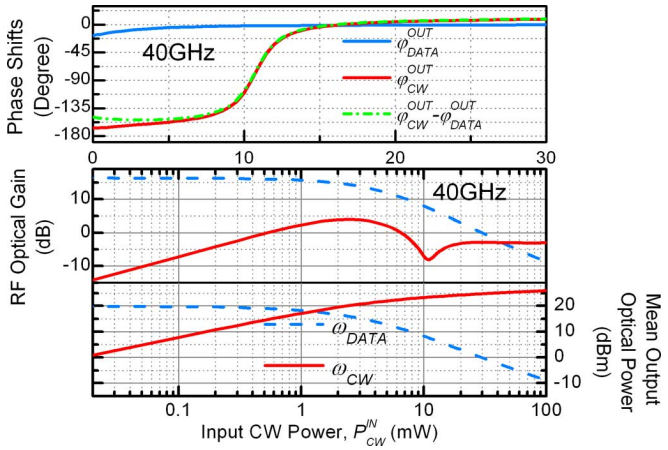

Fig. 3. Characteristics of the RF output signal at a current of 10 kA/cm^2. (Top) Phase shift. (Bottom) RF optical gain and mean output optical power as a function of input CW power. The input data signal power is 1 mW and has a 20% modulation index at a modulation frequency of 40 GHz.

the two lowest discrete QD bound states, i.e., excited (E) and ground (G) state, which are connected by fast (subpicosecond) intersubband electron relaxation. The frequency detuning ($\omega_{\mathrm{DATA}} - \omega_{\mathrm{CW}} = \omega_E - \omega_G$) is assumed much larger than the homogenous linewidth of the QDs, and thus FWM interaction between data and CW signals are neglected. Second, the input CW power $P^{\mathrm{IN}}_{\mathrm{CW}}$ is variable and acts as a strong pump, while the average input data power $P^{\mathrm{IN}}_{\mathrm{DATA}}$ is constant and relatively weak. Therefore, the dynamic gain grating is no longer solely determined by the data signal as in the small-signal regime. Instead, both the data and XGM-converted signal are considered to compete for the available carriers and interact with dynamic gain gratings (at frequencies ω_{DATA} and ω_{CW}) via XGM in terms of the two-wave competition.

The QD SOA's model is based on the rate equation approach originally developed for carrier dynamics in 1100-nm InAs–GaAs QDs [13], which describes the carrier scattering between QD subbands and Reservoir (R) including Wetting layer and barrier. Inhomogeneous gain broadening of self-assembled QDs and homogenous broadening of stimulated emission/absorption are included. A local carrier density description of QD bounded hole states with 100-fs valence intraband scattering time has been used. The maximum modal gain values are 24 cm^{-1} at the center of G state transition and 38 cm^{-1} at the E state peak. The device is 2 mm long and has an internal loss of 2 cm^{-1}. For the electron dynamics at strong current injection (10 kA/cm^2), the longest characteristic time scale ($\sim$0.7 ns) is the R state carrier lifetime, the intermediate time (2.5 ps) is the electron capture from R to E (or G) states, and the shortest time (0.2 ps) is the intradot electron relaxation from E to G states. These time scales were extracted from two-color pump–probe measurements [14] and many-body calculations [15]. Here, optical intensity propagation equations have been used and dispersive effects are not included. In this work, we emphasize the phase shifting profile of the XGM converted signal (ω_{CW}) after the QD SOAs for a strong current injection (10 kA/cm^2).

Fig. 2(left) shows the calculated static modal gain of QD SOAs for different values of the input CW power. As the stimulated emission at frequency ω_{CW} (input CW power) increases, spectral holes are seen to develop in the gain spectrum, centered at the E and G states. Notice that the spectral hole burning corresponding to the E state transition originates from the large contrast between the fastest intradot electron relaxation and the intermediate electron capture from R to E states, which is synonymous to the existence of an injection bottleneck due to long capture time or short escape time [16]. As the rate of removal of carriers in the QD G state due to stimulated emission approaches the injection rate between reservoir and QDs, it is possible to deplete the E state carrier population and thus even switch from gain to absorption. Now, in the presence of a modulated data signal, let us consider the modal gain at frequency ω_{CW} in the form of a Fourier series: $\overline{g} + \sum_{n=1}^{\infty}[|\Delta\tilde{g}_n|\exp(i2\pi nft + i\Delta\phi_n) + c.c.]/2$. Here, $\overline{g}$ is the static gain, and $|\Delta\tilde{g}_n|$ and $\Delta\phi_n$ are the modulated gain and phase for the nth order harmonics. In this letter, the modulation index of input data signal (ω_{DATA}) is fixed at 20%. As the higher order harmonics give small contributions (distortion) to the overall XGM, we only keep the first-order harmonics. The XGM response, $|\Delta\tilde{g}_1|/\left(P^{\mathrm{IN}}_{\mathrm{DATA}} m_0\right)$, and the relative phase, $\Delta\phi_1$, are shown in Fig. 2(right). Flat XGM responses approximately up to 100 GHz are observed, which reveals the role of fast intersubband QD carrier dynamics [11]. As the CW power is modest, the XGM responses in the low modulation frequency range have a phase shift of around $-\pi$ relative to the modulation of the input data signal, which is similar to wavelength conversion with an inverse pattern in the small signal regime [10]. As the CW power is strong and depletes the gain of E state into absorption, a π-shift of the XGM response is consistent with switching to "noninverting" cross-absorption modulation (XAM) [17]. Thus, by increasing the input CW power, the XGM converted signal experiences the corresponding π-shift and also benefits from the efficient conversion at high modulation frequencies.

III. Phase Profile in Wavelength Conversion

Fig. 3 shows the calculated characteristics of the RF output signal at a modulation frequency of 40 GHz in our wavelength conversion configuration under strong current injection. We fix the input data signal at 1 mW to retain a reasonable signal-to-

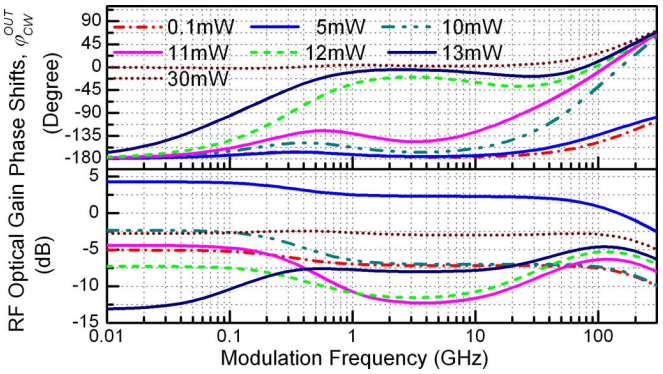

Fig. 4. Spectral characteristics of the XGM converted output signal for different input CW power at a current density of 10 kA/cm^2. (Top) Phase shift. (Bottom) RF optical gain. The input data signal is 1-mW input with 20% modulation index.

noise level. Fig. 3(top) shows a $\sim$180° tunable phase shift $\varphi_{\mathrm{CW}}^{\mathrm{OUT}}$ for the XGM converted output by controlling the input probe power. The sharp increase of the phase shift corresponds to the notch-type drop of the XGM efficiency (related to the RF optical gain) seen in Fig. 3(bottom) at frequency ω_{CW}. By evaluating the mean output optical power in Fig. 3(bottom), the wavelength conversion in QD SOAs can be divided into two regimes: a small-signal regime ($P_{\mathrm{CW}}^{\mathrm{OUT}} \ll P_{\mathrm{DATA}}^{\mathrm{OUT}}$) and a two-wave-competing regime (where $P_{\mathrm{CW}}^{\mathrm{OUT}}$ is comparable to or much larger than $P_{\mathrm{DATA}}^{\mathrm{OUT}}$). In the small-signal regime, only the data signal dominates the dynamic gain grating and a linear increase of XGM efficiency can be observed. The intensity envelopes of the output data signal and the XGM converted signal are nearly out of phase ($\sim$180° for $\varphi_{\mathrm{CW}}^{\mathrm{OUT}} - \varphi_{\mathrm{DATA}}^{\mathrm{OUT}}$). In the two-wave-competition regime, the dynamic gain gratings depend on the mean power of the spatially varying CW signal. As the stimulated emission at the G state transition reaches the maximum value imposed by the injection bottleneck, the amplifiers can be regarded as being spatially divided into a usual XGM section and an XAM section. Thus, the intensity envelope of the XGM signal experiences a π-shift in between these two sections, which results in a notch-type drop in the XGM efficiency and a $\sim$180° phase shift.

Fig. 4 shows the XGM converted output signal as a function of modulation frequency for different input CW power levels. Due to the fast intersubband carrier dynamics between E and G states, the dynamic gain grating (at frequencies ω_{DATA} and ω_{CW}) can balance and follow each other at high-speed modulation. It is seen that a shift of π can be achieved by changing the input power from 5 to 30 mW for modulation frequencies even beyond 100 GHz. For different modulation frequencies, different input power levels are required to achieve a given phase shift, such as $\pi/4$, $\pi/2$, $3\pi/4$, etc. We also notice that the corresponding RF optical gain changes significantly, which is an undesirable feature. This feature is related to the properties of the dynamic gain grating as a function of modulation frequency shown in Fig. 2(right). Especially in the two-wave-competition regime, the magnitude and phase of the XGM response vary for different modulation frequencies even for identical mean power. Therefore, the cancellation and reconstruction of the XGM converted signal (notch-type drop appearance of RF optical gain in Fig. 3) are sensitive to both modulation frequency and input CW power. In practice, there is a trade-off between the maximum modulation frequency and the minimum signal power to retain a reasonable signal-to-noise ratio.

IV. Conclusion

We numerically demonstrated a scheme to realize a $\sim$180° broadband microwave phase shifter based on high-speed XGM in QD SOAs under strong current injection. The modulation bandwidth is predicted to be beyond 100 GHz, limited by the fast intersubband carrier dynamics in QDs.

References

[1] C. Chang-Hasnain and S. L. Chuang, "Slow and fast light in semiconductor quantum-well and quantum-dot devices," *J. Lightw. Technol.*, vol. 24, no. 12, pp. 4642–4654, Dec. 2006.

[2] A. Matsudaira *et al.*, "Electrically tunable slow and fast lights in a quantum-dot semiconductor optical amplifier near 1.55 μm," *Opt. Lett.*, vol. 32, pp. 2894–2896, 2007.

[3] J. Mørk, F. Öhman, M. van der Poel, Y. Chen, P. Lunnemann, and K. Yvind, "Slow and fast light: Controlling the speed of light using semiconductor waveguides," *Laser Photon. Rev.*, vol. 3, pp. 30–44, 2009.

[4] F. Öhman, K. Yvind, and J. Mørk, "Slow light in a semiconductor waveguide for ture-time delay applications in microwave photonics," *IEEE Photon. Technol. Lett.*, vol. 19, no. 15, pp. 1145–1147, Aug. 1, 2007.

[5] W. Xue, S. Sales, J. Capmany, and J. Mørk, "Wideband 360° microwave photonic phase shifter based on slow light in semiconductor optical amplifiers," *Opt. Express*, vol. 18, pp. 6156–6163, 2010.

[6] M. R. Fisher and S. L. Chuang, "A microwave photonic phase-shifter based on wavelength conversion in a DFB laser," *IEEE Photon. Technol. Lett.*, vol. 18, no. 16, pp. 1714–1716, Aug. 15, 2006.

[7] T. Akiyama, M. Sugawara, and Y. Arakawa, "Quantum-dot semiconductor optical amplifiers," *Proc. IEEE*, vol. 95, no. 9, pp. 1757–1766, Sep. 2007.

[8] A. V. Uskov, E. P. O'Reilly, M. Laemmlin, N. N. Ledentsov, and D. Bimberg, "On gain saturation in quantum dot semiconductor optical amplifiers," *Opt. Commun.*, vol. 248, pp. 211–219, 2005.

[9] T. W. Berg, J. Mørk, and J. M. Hvam, "Gain dynamics and saturation in semiconductor quantum dot amplifiers," *New J. Phys.*, vol. 6, pp. 178-1–23, 2004.

[10] J. Kim, M. Laemmlin, C. Meuer, D. Bimberg, and G. Eisenstein, "Theoretical and experimental study of high-speed small-signal cross-gain modulation of quantum-dot semiconductor optical amplifiers," *IEEE J. Quantum Electron.*, vol. 45, no. 3, pp. 240–248, Mar. 2009.

[11] D. Nielsen *et al.*, "High-speed wavelength conversion in quantum dot and quantum well semiconductor optical amplifiers," *Appl. Phys. Lett.*, vol. 92, pp. 211101-1–3, 2008.

[12] G. Bramann, H.-J. Wunsche , U. Busolt, C. Schmidt, M. Schlak, B. Sartorius, and H.-P. Nolting, "Two-wave competition in ultralong semiconductor optical amplifiers," *IEEE. J. Quantum Electron.*, vol. 41, no. 10, pp. 1260–1267, Oct. 2005.

[13] T. W. Berg and J. Mørk, "Saturation and noise properties of quantum-dot optical amplifiers," *IEEE J. Quantum Electron.*, vol. 40, no. 11, pp. 1527–1539, Nov. 2004.

[14] I. O'Driscoll, T. Piwonski, C. F. Schleussner, J. Houlihan, G. Huyet, and R. J. Manning, "Electron and hole dynamics of InAs/GaAs quantum dot semiconductor optical amplifiers," *Appl. Phys. Lett.*, vol. 91, pp. 071111-1–3, 2007.

[15] T. R. Nielsen, P. Gartner, F. Jahnke, and A. A. Sawchuk, "Many-body theory of carrier capture and relaxation in semiconductor quantum-dot lasers," *Phys. Rev. B*, vol. 69, pp. 235314-1–13, 2004.

[16] M. Tessler, R. Nagar, and G. Eisenstein, "Structure dependent modulation responses in quantum-well lasers," *IEEE J. Quantum Electron.*, vol. 28, no. 10, pp. 2242–2250, Oct. 1992.

[17] N. Cheng and J. C. Cartledge, "Measurement-based model for cross-absorption modulation in an MQW electroabsorption modulator," *J. Lightw. Technol.*, vol. 22, no. 7, pp. 1805–1810, Jul. 2004.